ACS Catalysis

Research Article

pubs.acs.org/acscatalysis

Theoretical Studies on the Mechanism of Homogeneous Catalytic Olefin Hydrogenation and Amine−Borane Dehydrogenation by a Versatile Boryl-Ligand-Based Cobalt Catalyst

Gaurab Ganguly, Tanmay Malakar, and Ankan Paul*

Raman Center for Atomic, Molecular and Optical Sciences, Indian Association for the Cultivation of Science, Kolkata 700 032, India

Supporting Information

ABSTRACT: We have conducted mechanistic investigations using dispersion-corrected hybrid density functional theory on three different homogeneous processes: (a) hydrogenation of styrene using H_2, (b) dehydrogenation of amine−borane, and (c) transfer hydrogenation of styrene using amine−borane catalyzed by a boryl-ligated Co-based catalytic system, $LCo(N_2)$ (where L = meridional bis-phosphinoboryl (PBP) ligand), recently developed by Peters and co-workers (Lin, T.-P; Peters, J. C. *J. Am. Chem. Soc.* **2013**, *135*, 15310−15313). Our studies reveal that all three catalytic processes are facilitated by the same active species, which is of the form $LCo(H)_2$. The formation of the active catalytic species in turn determines the rate-determining barrier (RDB) for the hydrogenation reactions of the olefin and also for the dehydrogenation reaction of amine−borane. We predict that the RDB for hydrogenation of styrene under H_2 atmosphere is 17.3 kcal/mol, which occurs through a channel that involves switching of a singlet electronic ground state (S_0) of the organometallic catalytic species to its low-lying triplet electronic state (T_1) and returning back to the singlet surface through minimum energy crossing points along the reaction coordinate. Alternatively, we estimate the RDB to be 19.4 kcal/mol, slightly higher than that of the previous channel, if only the singlet spin state surface is considered. We find that the associated RDB for both the dehydrogenation of amine−borane (NMe_2H-BH_3) and transfer hydrogenation of styrene by amine−borane are higher than the hydrogenation of olefin using H_2(g) and is predicted to be 24.7 kcal/mol. In addition, we show that in the reaction involving amine−borane, the active catalytic species ($LCo(H)_2$) can get deactivated by forming a hydridoborane cobalt tetrahydridoborate complex, which happens through an S_N2 type nucleophilic attack by the $LCo(H)_2$ on amine−borane.

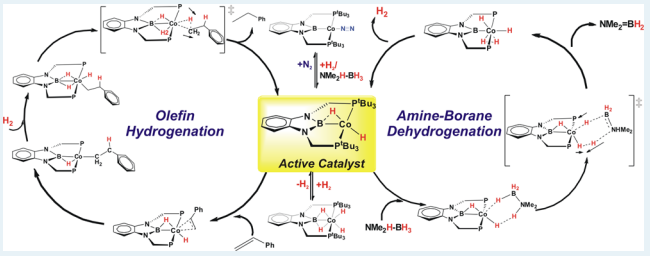

KEYWORDS: *cobalt catalyst, boryl ligand, spin−crossover, amine−borane dehydrogenation, olefin hydrogenation*

INTRODUCTION

The intriguing chemistry of transition metal (TM) complexes containing a pincer ligand as a backbone have emerged as a field of contemporary interest as a result of their vast applications in catalysis.[1−3] In particular, Ir pincer complexes containing PCP and PNP have been widely applied for various catalytic chemical transformations.[4,5] Further innovations have been directed toward modifying the pincer ligand backbone by incorporation of boron-based ligand into the pincer ligand framework. Not only have several TM−PBP complexes been synthesized but also their exciting chemistries have been unveiled over the past few years.[6,7] Depending upon the nature of the boron atom in the ligand scaffold, ligands can be broadly classified as borane, boryl, and borylenes, and their potential application in catalysis has been demonstrated.[8−13]

Understanding the nature of bonding between the transition metal center and the boron-supported ligand in these classes of complexes has garnered much attention over the past few decades.[14−17] The findings from extensive crystallographic, spectroscopic, and computational studies suggest that the bonding nature varies significantly with the valency of the boron center in the ligand backbone. For example, in the case of borane as a ligand backbone, the boron center acts as a Lewis acid and the TM center acts as a Lewis base center, and the interaction between the TM and the borane unit is limited to only σ type charge transfer.[14,15] On the other hand, in the boryl-based ligand backbone, the bonding interaction between the TM and the boryl (BR_2) unit is much stronger because along with the σ bond between the TM and the boryl moiety, there is a further π back-donation from the TM to the boron center as a result of the presence of an appropriate vacant p orbital on the B atom.[17−19]

Moreover, these important classes of boron containing TM complexes are known to activate dihydrogen (H_2) at room to moderate temperatures.[8,20] Interestingly, the mode of H_2 addition across the metal−boron linkage varies, depending upon the nature of the metal−boron bonding. For instance, in the case of the Ni−[$^{Mes}B(o\text{-}Ph_2PC_6H_4)_2$] complex recently

Received: September 9, 2014
Revised: February 27, 2015
Published: March 6, 2015

DOI: 10.1021/cs501359n
ACS Catal. 2015, 5, 2754−2769

prepared by Peters and co-workers,[8] which basically bears a TM−borane moiety, activation of H_2 along the Ni−borane unit is observed where the borane unit acts as a Lewis acid, the Ni center acts as a Lewis base center, and H_2 is heterolytically cleaved.[9] Of late, the same group has successfully demonstrated reversible H_2 activation along the Co−B bond in Nozaki's bisphosphinohydridoborane ligated cobalt in a typical TM−boryl complex.[20] However, such complexes are seldom used for H−H σ bond activation. They have achieved this feat at room temperature and stretched its catalytic activity into olefin hydrogenation.[20] Furthermore, they have shown that this particular catalyst can effectively dehydrogenate amine−borane (NMe_2H−BH_3), a very important class of molecules related to chemical hydrogen storage,[21−23] and can facilitate further hydrogenation of an olefin, thus acting as a transfer hydrogenation catalyst. Incidentally, this happens to be the first report on reversible H_2 activation by a first row TM catalyst. In addition, this is the first known instance of amine−borane dehydrogenation and transfer hydrogenation of olefin using amine−borane as transfer hydrogenating agent by a early TM complex.

Peters et al. further utilized the same PBP pincer ligand to prepare dinuclear Co and Ni complexes and catalyzed olefin hydrogenation using H_2(g).[24] These results clearly suggest that the boryl ligand plays an important role in all the above-mentioned chemical processes. Peters et al. were successful in isolating several in situ-generated intermediates in the catalytic hydrogenation process. However, the complete mechanistic scenario and electronic structure of several intermediates of hydrogen activation along with olefin hydrogenation by this Co-boryl complex is yet to be uncovered. Moreover, information about the actual catalytic species involved in the olefin hydrogenation and amine−borane dehydrogenation remains vague. In addition, there is a significant amount of interest in discovery of inexpensive, earth-abundant transition-metal-based homogeneous catalysts for olefin hydrogenation[8,20] and amine−borane dehydrocoupling for chemical hydrogen storage.[25−27] In particular, the mechanistic intricacies of amine−borane dehydrogenation have been under intense scrutiny from both the experimental and the theoretical community.[28−30]

Theoretical investigations by Paul and Musgrave revealed that ammonia−borane (NH_3−BH_3) dehydrogenation in the presence of Ir-pincer catalyst [POCOP ^{t}BuIr(H)$_2$] happens through a concerted N−H and B−H abstraction mechanism.[31] Similar concerted proton and hydride removal in the case of ammonia−borane dehydrogenation by Ni(NHC)$_2$, in which active participation of NHC ligand has been implicated, has also been predicted.[32] In contrast, Hall and co-workers have proposed a noninnocent NHC-ligand-based N−H-activation-initiated ammonia−borane dehydrogenation pathway.[33] Stepwise dehydrocoupling of ammonia−borane in which the B−H activation is followed by the N−H activation has also been reported by Ohno et al.[34] Ammonia−borane dehydrogenation via B−H activation prior to N−H activation has been described by Baker et al.[35] and Weller et al.,[36] as well. Hence, the mechanistic features of dehydrogenation of amine−boranes is an interesting area of contemporary research. The boryl ligand framework in the Co-boryl complex devised by Peters et al.,[20] because of its unique electronic disposition, can have a significant role in amine−borane dehydrogenation and transfer hydrogenation of alkene using amine−borane. Motivated by these factors, we have conducted theoretical investigations with dispersion-corrected hybrid density functional techniques (DFT) to unravel the molecular details of this catalytic transformation. Herein, using DFT, we have investigated the reactions shown in Scheme 1 in detail with all alternative intermediates and transition states and have unearthed crucial facets of these catalytic reactions.

Scheme 1. Chemical Processes That Will Be Explored Computationally in This Work

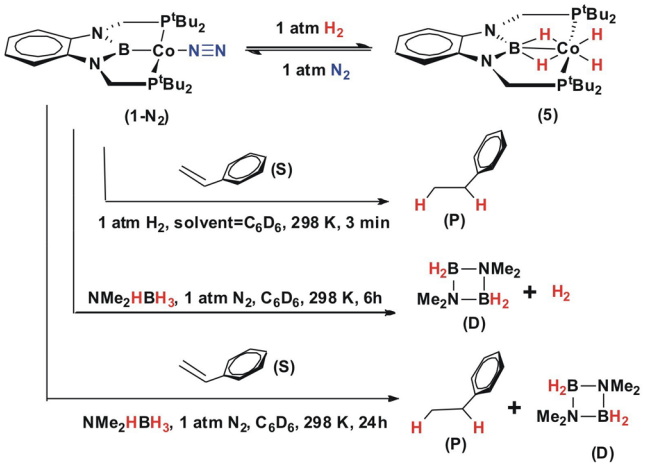

COMPUTATIONAL DETAILS

All calculations were conducted using the DFT[37,38] method by using the Gaussian09, A.02 revision[39] suite of programs. All gas phase geometry and transition states were optimized using the B3PW91 functional[9,40−43] with empirical dispersion added to it (B3PW91-D). This functional contains both exact exchange and dispersion corrections that play important roles in correctly describing weak interactions. To incorporate the dispersion interactions empirically, the keyword "IOp(3/124=3)" has been used.[44] This particular choice of IOp sets the S6 value of 1.0 for B3PW91 instead of 1.05, as suggested by Grimme, to take into account the dispersion interactions empirically.[45,46] The B3PW91 functional was chosen as benchmarking studies of functionals with transition metal compounds indicate that B3PW91 can be considered to be a reliable tool for studying transition metal chemistry.[47,48] Furthermore, the B3PW91 functional has been extensively used for understanding the electronic structure of organometallic cobalt complexes[49,50] and the mechanism of reactions facilitated by cobalt complexes[49−52] and also for molecular electronic applications.[53]

The recent studies from Grimme's group has strongly suggested that it is important to include empirically dispersion corrections with these regularly used functionals.[54] Moreover, the inclusion of Grimme's empirical dispersion correction has been shown to be crucial for bulky catalysts because it helps in accurate predictions of reaction barriers.[55] The all-electron 6-31++G(d,p) basis was used for boron, nitrogen, phosphorus, the H_2 molecule, all atoms of the styrene (**S**), and all atoms of NMe_2H−BH_3 (**AB**) and 6-31G(d) basis for rest of the atoms. The effective core potentials of the Stuttgart−Dresden−Bonn group were employed for the core electrons of the cobalt center, and the (311111/22111/411/1) basis set was used for its valence electrons[56] (this combination of basis on Co center is denoted as SDB basis set). This basis set combination is denoted as BS1.

DOI: 10.1021/cs501359n
ACS Catal. 2015, 5, 2754−2769

Harmonic vibrational frequencies were calculated in the gas phase with the BS1 basis set to identify intermediates with no imaginary frequency and transition states (TS) with only one imaginary frequency. The single-point electronic energy in the solvent phase (solvent = C_6D_6) was calculated with the B3PW91-D functional with all-electron 6-31++G(d,p) for nonmetal atoms and SDB basis set on the cobalt center. This basis set combination is denoted as BS2. Solvation effects were evaluated by the conductor-like polarizable continuum model (CPCM)[57,58] with UFF radii, where the optimized structures in the gas phase with BS1 basis set were employed.

Thermal corrections and entropy contributions to the Gibbs energy were incorporated from the gas phase frequency calculations at 1 atm pressure and 298 K. For solvent-phase entities, the entropy used for estimating solvent-phase free energies was derived by scaling the corresponding gas-phase entropies computed using the ideal-gas model by a factor of 0.5. This is a standard approximation that has been used in other quantum chemical studies.[59−62] For H_2(g) and N_2(g), we have taken the gas phase entropy (1.0 scaling factor applied to entropy obtained from gas phase quantum chemical model). To check the reliability of the results predicted by the B3PW91-D functional, we did single-point solvent-phase calculations using the CPCM model with some other widely used density functionals, such as B3LYP, M06, M06L, ωB97XD, TPSSh, LC-ωPBE, etc., on certain crucial intermediates and transition states obtained from B3PW91-D/BS1 gas-phase geometry optimizations. Please note, for computing solvent-phase free energies for these range of DFT functionals, the thermal corrections and entropy contributions to the Gibbs energy were taken from the gas phase frequency calculations done at B3PW91-D/BS1 level of theory.

The D3 version of Grimme's dispersion correction with the original D3 damping function[63] was also included with the B3PW91, B3LYP, M06, M06L, and LC-ωPBE functionals with the keyword "EmpiricalDispersion=GD3", which is available in the Gaussian 09, D.01 revision. Furthermore, geometry optimizations and frequency calculations were performed on some important intermediates and transition states using B3PW91-GD3 and ωB97XD functionals to check the effect of different functionals on the optimized geometries. The free energy profiles plotted with different GGA and meta-GGA functionals with and without Grimme's D and D3 dispersion correction are provided in the Supporting Information. In addition, a note and table on the performance evaluation of the different functionals is provided in the Supporting Information.

RESULTS AND DISCUSSION

To get a complete grip of the mechanistic intricacies, the actual Co-catalyst (**1-N_2**) without any truncation as was originally employed by Peters and co-workers[20] was used in our investigations. Styrene was chosen as the model reactant. We break down our discussion on systematic DFT investigation broadly into three parts: (I) First, we discuss the mechanism of hydrogenation of the Co-catalyst itself in 1 atm H_2 pressure, (II) then we move on to the catalytic hydrogenation of **S** by using gaseous molecular H_2(g), and finally, (III) we shed light on the mechanistic pathways of the catalytic hydrogenation schemes of **S** in the presence of amine−borane (**AB**) as a transfer hydrogenating agent. The ensuing text discusses the relative solvent phase Gibbs free energy changes and free energy activation barriers calculated using the B3PW91-D functional on the singlet potential energy surface until and unless mentioned otherwise.

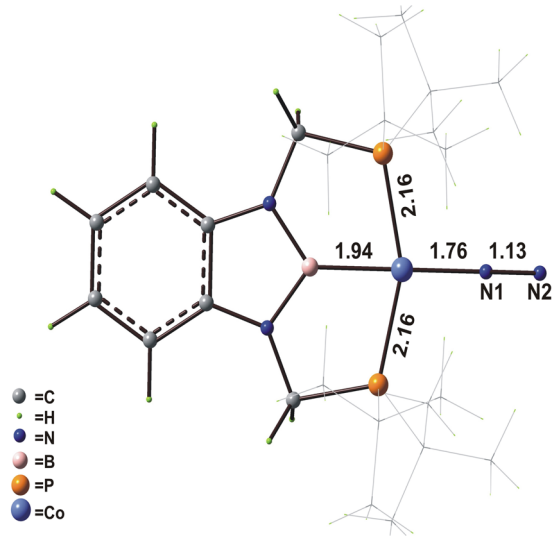

Figure 1. Optimized geometry of **1-N_2**. All bond lengths are given in angstroms.

I. Co-Boryl-Unit-Mediated H−H σ-Bond Activation. The ground state of the catalyst **1-N_2** is predicted to be a singlet (S_0). The corresponding triplet state (T_1) lies 17.6 kcal/mol higher than the ground singlet state. Around the square-planar Co center in the optimized geometry of the starting intermediate **1-N_2** (as shown in Figure 1), the dinitrogen (N_2) moiety lies trans to the boryl ligand, and the two phosphorus atoms are trans to each other. Our mechanistic investigations of H_2 activation by **1-N_2** under 1 atm H_2 pressure reveal two distinct pathways, namely, (i) a N_2 dissociative pathway and (ii) a H_2 associative pathway. These two pathways are discussed in detail below.

(i). N_2 Dissociative Pathway. In the N_2 dissociative channel, N_2 dissociation from the Co center forms a reactive tricoordinated species (**1**). Interestingly, the triplet state of **1** (which is denoted as **1′**) is predicted to be 5.6 kcal/mol more stable compared with that of the singlet state (**1**). Thus, it is evident that upon N_2 detachment, the catalyst changes its spin state from the singlet to the triplet state. This type of spin-forbidden ligand dissociation is fairly common in the area of organo-transition metal chemistry.[64,65] Experimentally, the hydrogenation of the **1-N_2** catalyst is unexpectedly fast in the solvent phase under 1 atm H_2 pressure. This can possibly arise as a result of the spin-forbidden N_2 dissociation to a triplet state (**1′**), occurring with a lower free energy barrier compared with the corresponding spin-allowed dissociation in the singlet state (**1**). However, such singlet (S_0, **1**)-to-triplet (T_1, **1′**) intersystem crossing (ISC) can be facilitated by spin orbit coupling due to the presence of the relatively heavy nucleus of Co (Z = 27). This prompted us to study the crossing between the singlet and triplet potential energy surfaces (PESs) of **1-N_2** along the N_2 dissociation reaction coordinate (RC) from the Co center. The partial optimization method along the RC (see the Supporting Information), which is very frequently used to locate the crossing between S_0 and T_1 surfaces, is employed here prior to identification of the exact minimum energy crossing point (MECP).[64,66−68] This method involves multiple geometry optimizations on the singlet and triplet PESs while keeping the Co−N1 distance constant. The two curves cross

DOI: 10.1021/cs501359n
ACS Catal. 2015, 5, 2754−2769

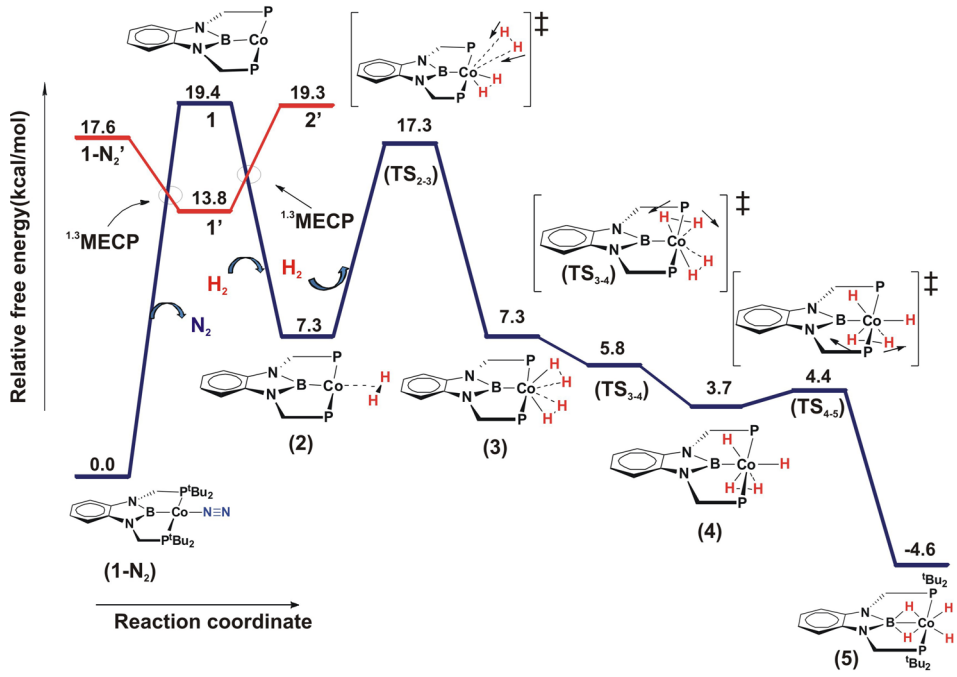

Figure 2. Free energy profile for hydrogenation of **1**-N_2 to form $LCo(H)_4$ (**5**) via $LCo(H_2)$ (**2**) through the N_2 dissociative channel. Red, triplet surface; blue, singlet surface.

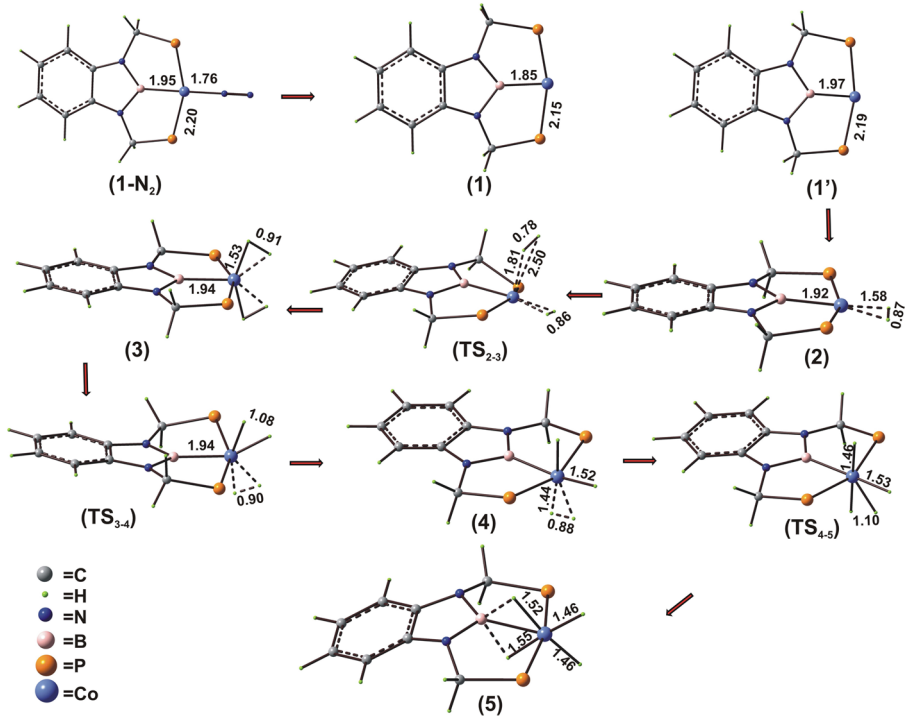

Figure 3. Optimized geometries of crucial intermediates and transition states involved in Figure 2. Key bond lengths are given in angstroms, and *tert*-butyl groups are omitted for clarity.

near a fixed Co−N(1) distance of 2.4 Å (see the Supporting Information). Single-point energy computations for each spin state at the partially optimized geometry of the other spin state predicts higher energies, 18.9 and 20.2 kcal/mol for the singlet and the triplet spin state, respectively. Then to explicitly locate the exact, full dimensional MECP, we have used the code written by Harvey et al. interfaced with Gaussian09 at the DFT level of theory.[69] The MECP point is predicted to be 15.4 kcal/mol higher in free energy than with respect to **1**-N_2.

After N_2 dissociation in the triplet state, one H_2 molecule can easily coordinate to the vacant position of the Co center to form intermediate **2**. The ground electronic state of **2** turns out to be singlet. Thus, binding of H_2 to **1**′ would proceed through another MECP between triplet and singlet PESs (see the Supporting Information). The free energy change (ΔG^0) of the

DOI: 10.1021/cs501359n
ACS Catal. 2015, 5, 2754−2769

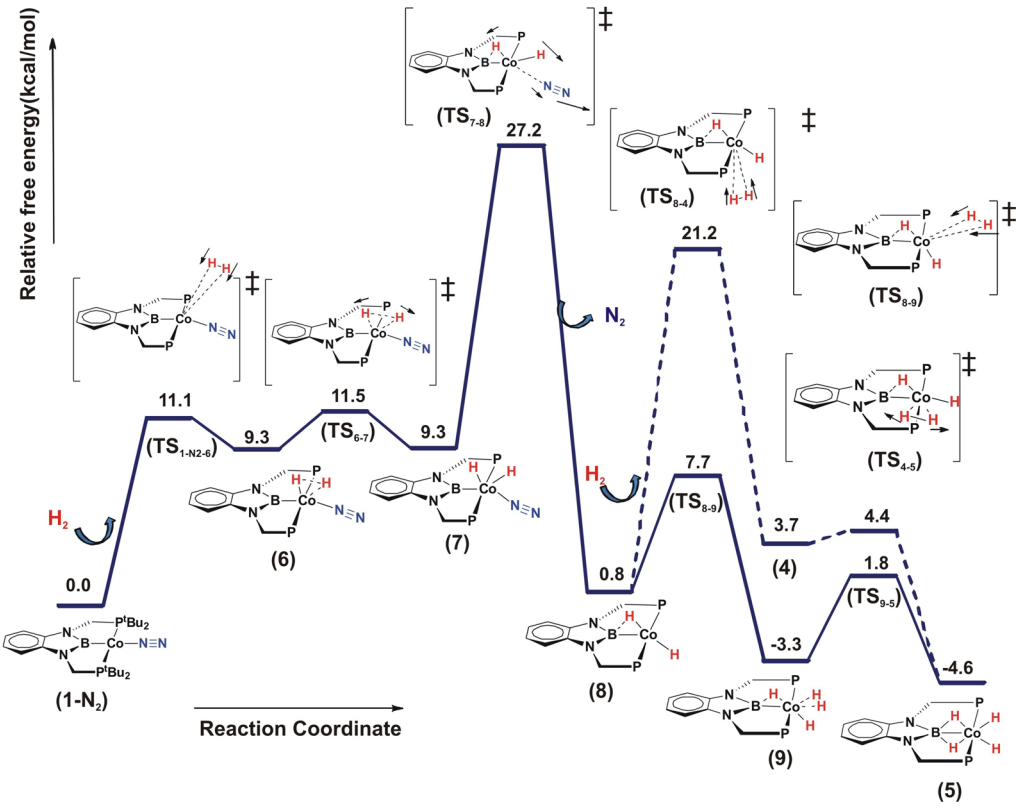

Figure 4. Free energy profile for hydrogenation of **1-N$_2$** to form **5** via LCo(H)$_2$ (**8**) through the H$_2$ associative channel.

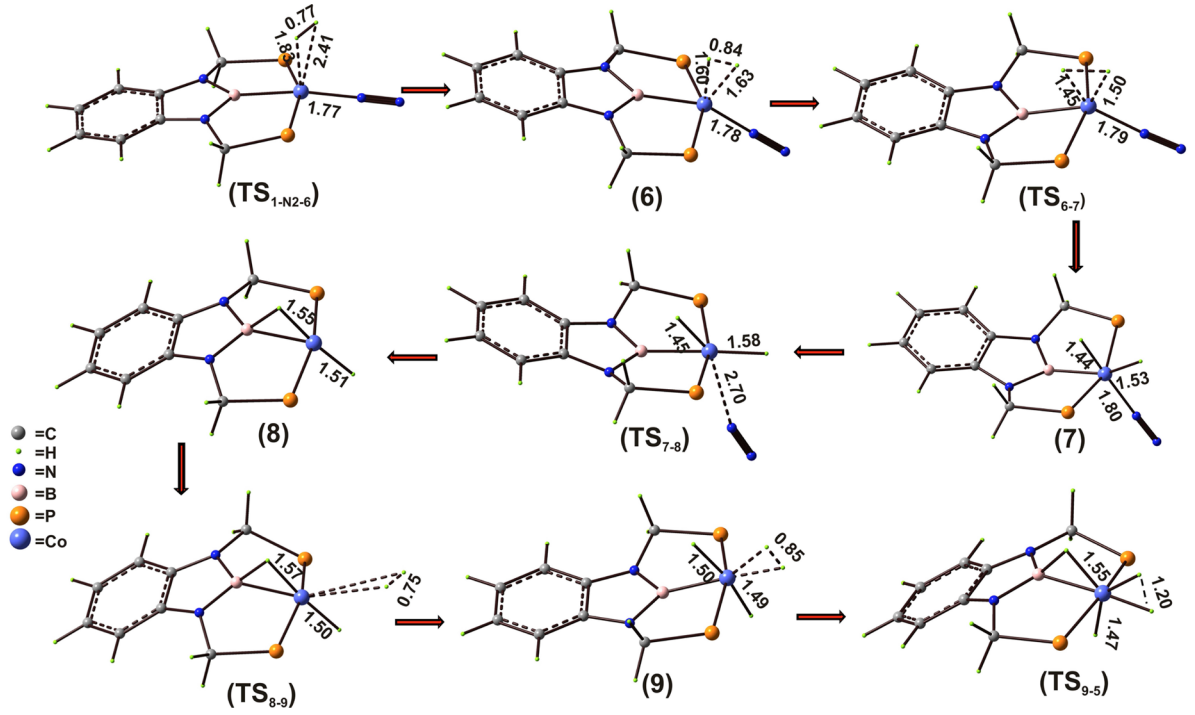

Figure 5. Optimized geometries of crucial intermediates and transition states involved in Figure 4. Key bond lengths are given in angstroms, and *tert*-butyl groups are omitted for clarity.

forward reaction LCo(N$_2$) (**1-N$_2$**) + H$_2$(g) = LCo(H$_2$) (**2**) + N$_2$(g) is estimated to be 7.3 kcal/mol (see Figure 2). The only possible coordination mode of H$_2$ to the Co center in **2** is the dihydrogen moiety (H$_2$) binding to the metal in the same plane as the boryl ligand backbone. We have also investigated alternative coordination modes of H$_2$ to the Co center. The other possible binding mode of H$_2$ does not lead to any true intermediate. The perpendicular mode of H$_2$ to the plane of the catalyst (**2″**) gives an imaginary mode (422*i*).

DOI: 10.1021/cs501359n
ACS Catal. 2015, 5, 2754−2769

Scheme 2. Proposed Schematic Representation for the Reversible Conversion of 1-N_2 to 5 and Generation of 8 from 5 upon Self-Dehydrogenation and the Associated Free Energy Profile for Generation of 8 from 5

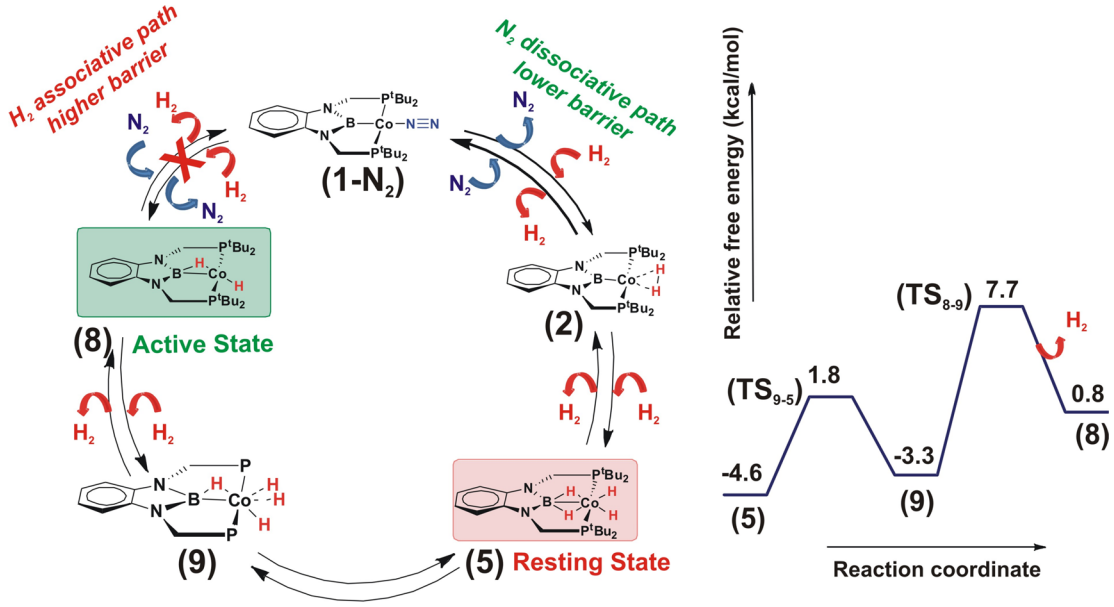

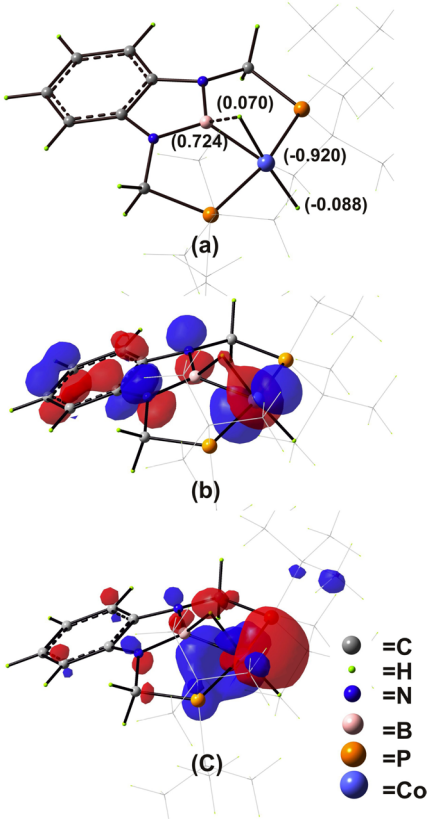

Figure 6. (a) NBO charge analysis of **8**, (b) HOMO of **8**, (c) LUMO of **8**.

Despite several attempts, we have failed to locate any intermediate in which the coordinated dihydrogen moiety is dissociated in the same plane of the catalyst over the Co center. Our findings suggest that splitting or activation of the singly coordinated H_2 is not possible on the Co center. Thus, we explored the prospect of further H_2 addition to **2**. Species **2** can bind another H_2 molecule, which leads to formation of complex **3**, in which two H_2 molecules coordinate in η^2 fashion to the Co center (see Figure 3). The associated free energy activation barrier ($\Delta G^{0‡}$) for generation of **3** is estimated to be 17.3 kcal/mol (see Figure 2). Complex **3** has a plane of symmetry (C_s), and the two H_2's coordinated to the metal center are equivalent.

The σ bond of one of the two dihydrogen moieties coordinated to the Co center can easily cleave on the Co center through $\mathbf{TS}_{3-4}$ to produce intermediate **4**. The transformation of **3** to **4** is predicted to be barrierless and exergonic by 3.6 kcal/mol. Following this, the second coordinated H_2 gets activated through $\mathbf{TS}_{4-5}$ on the Co center, and thus, a stable complex $LCo(H)_4$ (**5**) is produced. The hydrogenation of **1-N_2** to yield **5**, is exergonic by 4.6 kcal/mol. Thus, in the N_2-dissociative route, the dihydrogen activations followed by hydrogenations of the **1-N_2** to form the molecular entity **5** happen with a rate-determining Gibbs free energy barrier (RDB) of 17.3 kcal/mol, if we take into consideration the switching of spin states along the reaction path. The predicted RDB for transformation of **1-N_2** to **5** would be 19.4 kcal/mol if we consider only the singlet surface for this reaction.

(ii). H_2 Associative Pathway. In the H_2 associative channel, the catalyst (**1-N_2**) does not undergo any change of spin state along the RC and remains in the singlet spin state (S = 0) throughout. We found that a H_2 molecule can bind to the Co center of **1-N_2** in η^2 fashion prior to N_2 dissociation and forms an intermediate, **6**. Ligation of the dihydrogen molecule proceeds through $\mathbf{TS}_{1-N2-6}$ with an associated free energy activation barrier of 11.1 kcal/mol. In the next step, the η^2-ligated H_2 dissociates into two hydrides via $\mathbf{TS}_{6-7}$ and leads to the appearance of species **7**. Conversion of **6** to **7** is thermoneutral, and the associated $\Delta G^{0‡}$ due to $\mathbf{TS}_{6-7}$ is estimated to be 11.5 kcal/mol (see Figure 4). In **7**, N_2 is still coordinated to the Co center, and the Co center essentially has an octahedral arrangement of ligands. Further binding of a H_2 molecule to **7** does not happen because the Co center in **7** is well saturated. N_2 dissociation from **7** occurs through $\mathbf{TS}_{7-8}$.

DOI: 10.1021/cs501359n
ACS Catal. 2015, 5, 2754−2769

Scheme 3. Shematic Representation of Styrene Hydrogenation under 1 atm H_2 Pressure

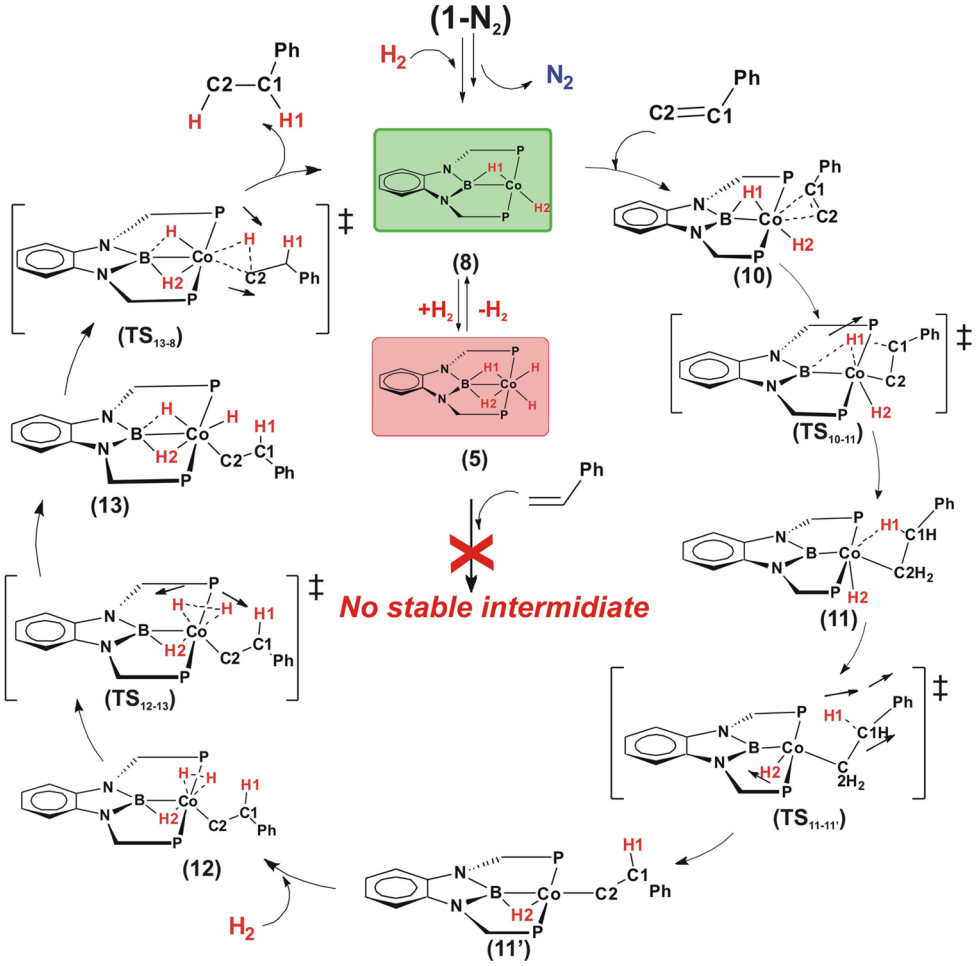

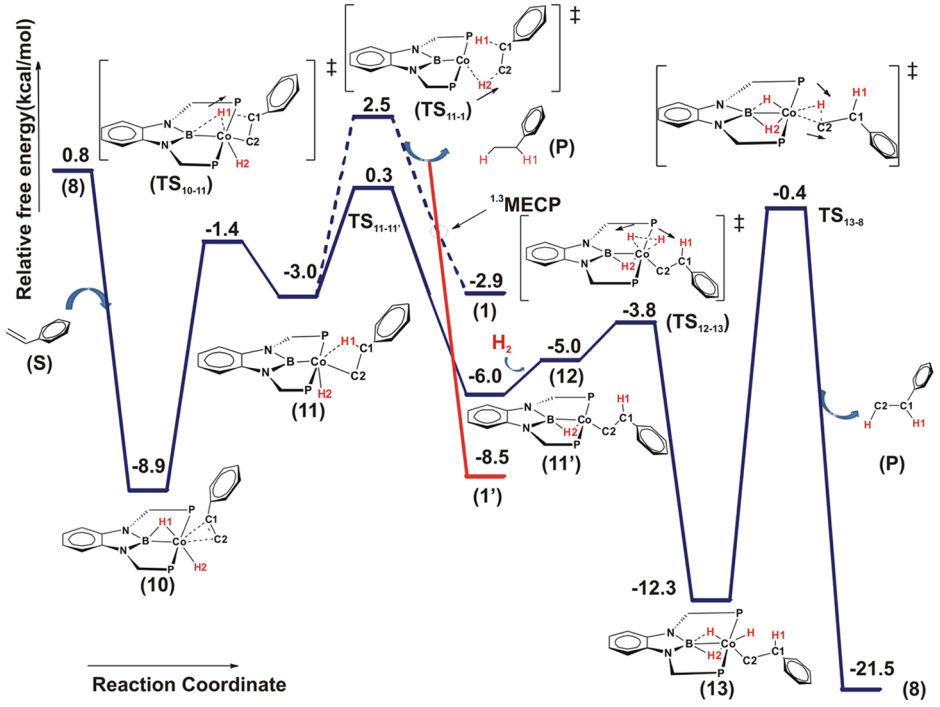

Figure 7. Free energy profile for styrene hydrogenation under 1 atm H_2 pressure. Red, triplet surface; blue, singlet surface.

DOI: 10.1021/cs501359n
ACS Catal. 2015, 5, 2754−2769

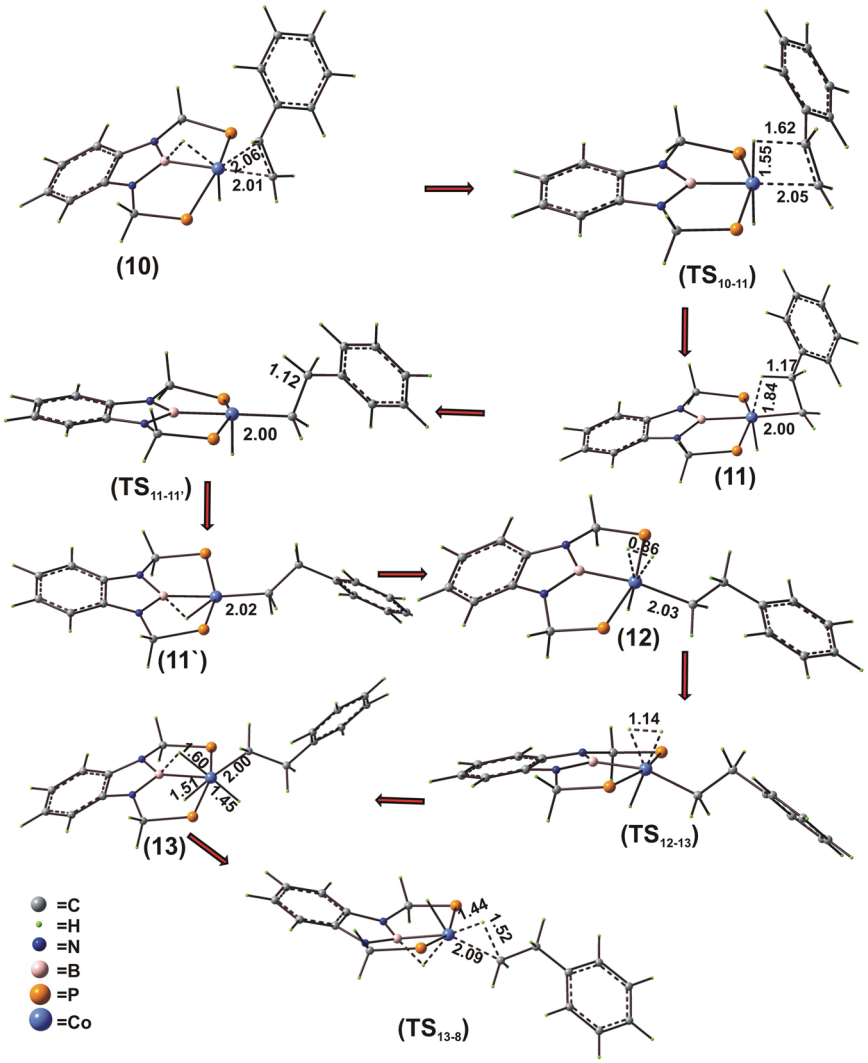

Figure 8. Optimized geometries of crucial intermediates and transition states involved in Figure 7. Key bond lengths are given in angstroms, and *tert*-butyl groups are omitted for clarity.

The dissociation of N_2 through TS_{7-8} is predicted to happen with $\Delta G^{0‡}$ of 27.2 kcal/mol and produces intermediate **8**. Notice that in the N_2 dissociative channel, formation of intermediate **8** was not observed upon single molecular dihydrogen (H_2) activation. Unlike the other dihydrogen complexes of such pincer ligands[31,70,71] the H−Co−H bond angle in **8** is predicted to be a higher one (see Figure 5). This is simply because of the presence of the boryl unit in the supporting ligand scaffold as it leads to bridging of the hydrogen between the Co and B center. It is clear from the geometry of **8** that it is coordinatively unsaturated and it can bind another molecule of H_2. The second molecule of H_2 can ligate to **8** in two different ways, cis and trans (see Figure 4). The *trans*-dihydrogen/dihydride complex (*trans*-$Co(H)_2(H_2)$) (**9**) is predicted to be more stable than the corresponding *cis*-dihydrogen/dihydride complex (*cis*-$Co(H)_2(H_2)$) (**4**) by 7.0 kcal/mol (see Figure 4). Hence, further hydrogenation of **8** through **9** is preferred. The ligated H_2 to the Co center in **9** and **4** gets activated with a barrier of 5.1 and 0.7 kcal/mol for the trans and cis isomers, respectively, to end up with the formulation of the experimentally observed species $LCo(H)_4$. Transformation of **8** to **5** is only 5.4 kcal/mol thermodynamically downhill. Thus, in the H_2 associative pathway, the RDB for hydrogenation of Co-catalyst is 27.2 kcal/mol. Comparison of the RDBs of the two aforementioned channels clearly indicates that the experimentally observed intermediate probably is formed through the N_2 dissociative pathway because it has a significantly lower barrier (17.3 kcal/mol) compared with the H_2 associative route (27.2 kcal/mol).

II. Catalytic Olefin Hydrogenation Using 1-N_2 under 1 atm H_2 and Room Temperature. The experimental findings of Peters et al. show that the olefin hydrogenation is extremely rapid with the Co complex under 1 atm H_2 pressure and room temperature.[20] However, the molecular form of the active catalytic species is not known. Initially, we thought **5** might be the active catalytic species in hydrogenating **S**, but we failed to trace any intermediate between **5** and the vinyl group of **S**. Interestingly, our aforementioned catalyst hydrogenation mechanism indicates that the catalyst can easily switch between dihydridoborato cobalt dihydride (**5**) and cobalt *trans*-dihydride dihydrogen form (**9**). The $\Delta G^{0‡}$ of self-dehydrogenation of **9** to generate the monohydrogenated species **8** is 11.0 kcal/mol (see Figure 4), which is comfortably accessible under the reported experimental conditions. Therefore, under H_2 atmosphere, the monohydrogenated form $LCo(H)_2$ can be generated from the dihydrogenated form $LCo(H)_4$ (**5**) by simple loss of H_2.

DOI: 10.1021/cs501359n
ACS Catal. 2015, 5, 2754−2769

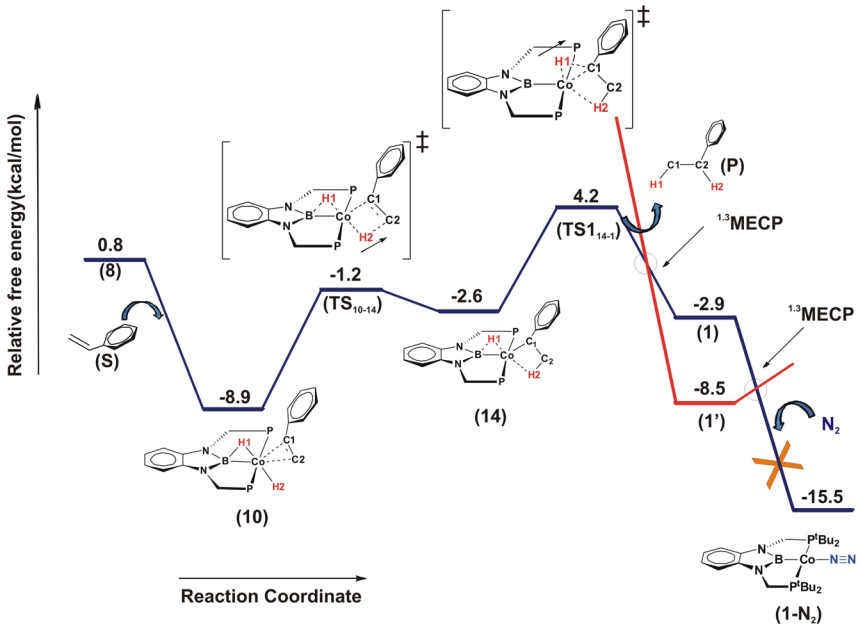

Figure 9. Free energy profile for the alternative route for styrene hydrogenation under 1 atm H_2 pressure. Red, triplet surface; blue, singlet surface.

Because **5** is the most stable hydrogenated form of the Co organometallic complex in the presence of H_2, it is probably the resting state of the catalyst.

Our studies reveal that the experimentally observed transformations under 1 atm H_2 pressure initiate with conversion of **1-N$_2$** to **2** as a result of the loss of one N_2 and addition of one H_2 (associated barrier = 13.8 kcal/mol), then **2** gets transformed to **5** with few interdediates in between. The rate-determining step for this transformation is 17.3 kcal/mol, which is associated with **TS$_{2-3}$**. Compound **5**, in turn, can generate **8** via self-dehydrogenation, with the intermediate being **9** (see Scheme 2). Note that **8** is not essentially formed upon single H_2 addition to **1**′ in the "N_2 dissocitive channel"; however, **8** can be generated during olefin hydrogenation by means of self-dehydrogenation of **5** via **9** after formation of **5** through the "N_2 dissociative channel". The sequence of these transformations is shown in Scheme 2.

It turns out that **8** can bind the vinyl group of **S**. In addition, **8** facilitates the hydrogenation of **S**. Therefore, **8** is the active form of the catalyst. However, **8** is 5.4 kcal/mol endoergic with respect to **5**, and **8** is not likely to be observed in an experimental setup because of its low population during the reaction. The unsaturation in the coordination sphere of the Co center in **8** is conducive for binding of the vinyl moiety of styrene (**S**) to the metal center and leads to the formation of **10**. Recall that H_2 can bind to **8** in a similar fashion to produce **5** (see Figure 4), but the relative gain in stability on olefin binding over that for H_2 binding to **8** is 5.6 kcal/mol. Hence, one can infer that there is a dynamic equilibrium between **10** and **9**, and the equilibrium is slightly favored toward **10**. These findings are in sound agreement with the experimental observation by Peters et al. that a trace amount of **5** was obtained along with ethylbenzene (**P**) in the reaction mixture.[20] Our investigations reveal that **8** is catalytically active and can facilitate hydrogenation of styrene; **8** is also identified as the catalytic active species for **AB** dehydrogenation, which will be discussed later in this article. The natural bond orbital (NBO) charge analysis of **8** predicts two distinct types of H atom over the Co center. The terminal hydrogen is hydridic in nature, and the bridged hydrogen is protic in nature. The frontier molecular orbitals of **8** shows significant contribution from the metal d orbitals in both HOMO and LUMO (see Figure 6). We envisaged two competing channels for olefin hydrogenation involving the active participation from species **8**. The theoretically predicted catalytic cycles are shown in Scheme 3.

The catalytic process initiates through the binding of the vinyl group of styrene to the Co center of **8** to form a stable intermediate, **10**. No transition state exists for this binding process. Hence, it is practically barrierless. In the next step, the bridging H (H1) atom between the B and Co is transferred to one of the carbon atoms (C1) of the vinyl moiety of styrene through **TS$_{10-11}$** (see Figure 7). It is clear from the optimized C−H bond length in **11** that the C1−H1 bond is activated in **11** (shown in Figure 8). The reverse C−H activation of C1−H1 and the simultaneous transfer of the terminal hydrogen atom H2 to a bridge atom position between the B atom the transition metal center can occur via **TS$_{11-11'}$** to lead to a more stable conformer (**11**′).

The $\Delta G^{0\ddagger}$ for this reaction is predicted to be 9.2 kcal/mol with respect to **10**. In **11**, the terminal hydrogen atom H2 can be simultaneously transferred to the C2 carbon of the **S**, leading to the direct formation of ethylbenzene **P** via **TS$_{11-1}$**. The associated free energy barrier of the transition state is predicted to be 11.4 kcal/mol with respect to **10**. A bare tri-coordinated catalyst (**1**) is generated initially in the S_0 state along with the ethylbenzene in this process, and then through ISC, **1** converts to the T_1 state (**1**′), which is lower in energy by 5.4 kcal/mol than the corresponding singlet state. Alternatively, a second equivalent of H_2 can bind to **11**′ to produce **12**. Binding of the second equivalent H_2 is endoergic by be 2.2 kcal/mol with respect to **11**′. The coordinated H_2 can easily split over the Co center through **TS$_{12-13}$** and leads to the formation of **13**. The formation of **13** from **8** is predicted to be exoergic by 11.5 kcal/mol. From **13**, ethylbenzene can be generated through the reductive elimination (**TS$_{13-8}$**). The free energy of activation for the reductive elimination is 11.9 kcal/mol with respect to **13**. In this particular channel, the ultimate alkane (**P**) formation

DOI: 10.1021/cs501359n
ACS Catal. 2015, 5, 2754−2769

Scheme 4. Proposed Catalytic Cycle for Catalytic AB Dehydrogenation

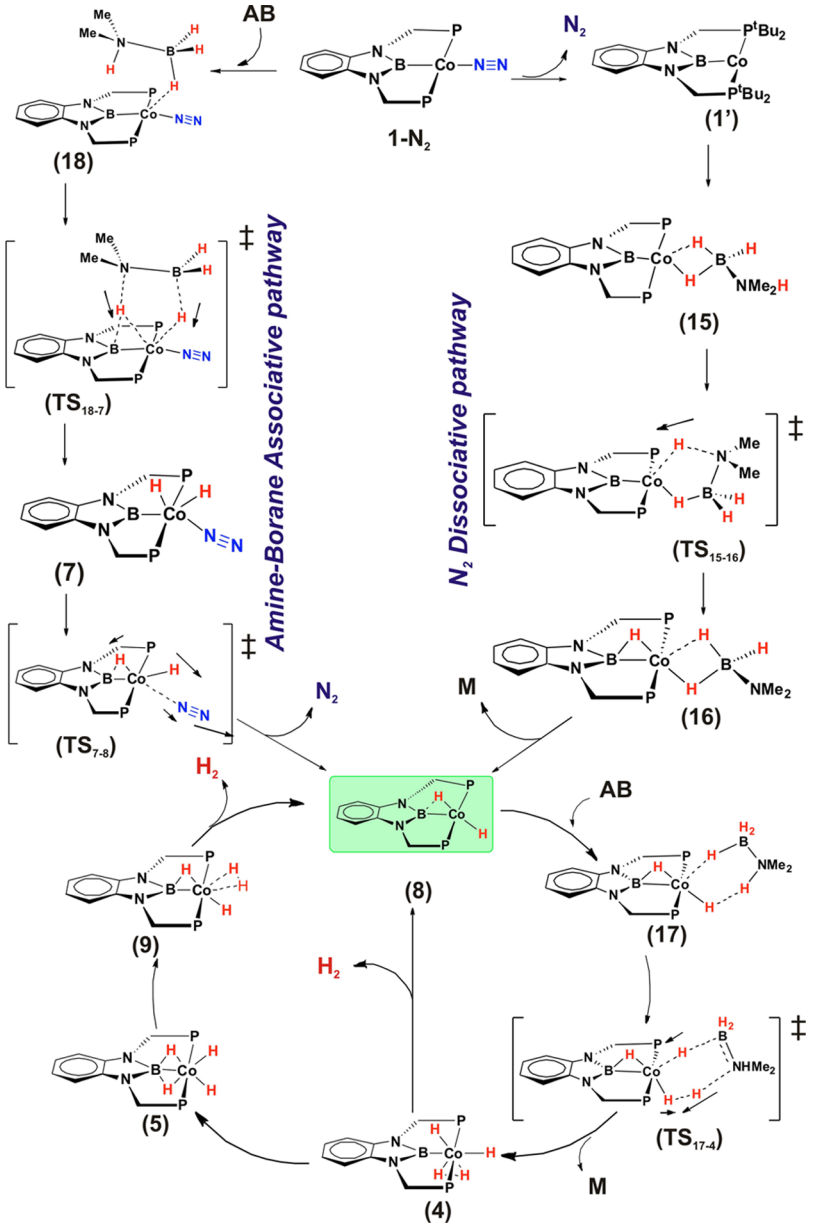

is thermodynamically favorable, and thus, the catalytically active species **8** is again regenerated during the course of this reaction.

An alternative channel exists in which, first, the vinyl group of **S** is inserted into the Co−H2 bond of **10** and then through $\mathbf{TS}_{10-14}$ yields intermediate **14**. The free energy of activation of this reaction is estimated to be 7.7 kcal/mol with respect to **10**, and the formation of **14** is exoergic with respect to **8** by 3.4 kcal/mol. This Co−H2 bond activation is thermodynamically comparable with the Co−H1 bond activation by the styrene. Further addition of a H_2 molecule to **14** is not possible, so after that, the H1 is transferred to the C1 through $\mathbf{TS}_{14-1}$ to form ethylbenzene, and simultaneously, the tricoordinated reactive species in its triplet state (**1**′) is generated. Because this alkene hydrogenation is done under a constant 1 atm H_2 pressure, N_2 is unlikely to bind to **1**′ to stabilize it and bring it back to the singlet state by forming **1-N$_2$**; however, under a H_2 atmosphere, **1**′ can further bind H_2, as described in Figure 1, and regenerate **8** for further olefin hydrogenation. By comparing both the reaction channels, it clearly turns out that the RDB of the reaction sequence shown in Figure 7 (11.9 kcal/mol) is slightly lower than the RDB of reaction channel presented in Figure 9 (13.1 kcal/mol), and under 1 atm H_2 pressure, the thermodynamically more favorable catalytic cycle would be the cycle described in Scheme 3.

III. Amine−Borane (AB) Dehydrogenation Using 1-N$_2$ and Transfer Hydrogenation. To figure out the mechanistic scenario of dehydrogenation of $NMe_2H{-}BH_3$ (**AB**), we found two distinct possibilities emanating from species **1-N$_2$**: (i) a N_2 dissociative pathway and (ii) an **AB** associative pathway.

(i). N_2 Dissociative Pathway. As discussed earlier, we witness the change in spin state from singlet to triplet along the N_2 dissociation reaction coordinate of **1-N$_2$** (as shown in Scheme 4).

Coordination of an **AB** molecule through its nucleophilic B−H end to **1**′ initially generates a species that is in its triplet state, and after passing through a MECP, it converts to a more stable

DOI: 10.1021/cs501359n
ACS Catal. 2015, 5, 2754−2769

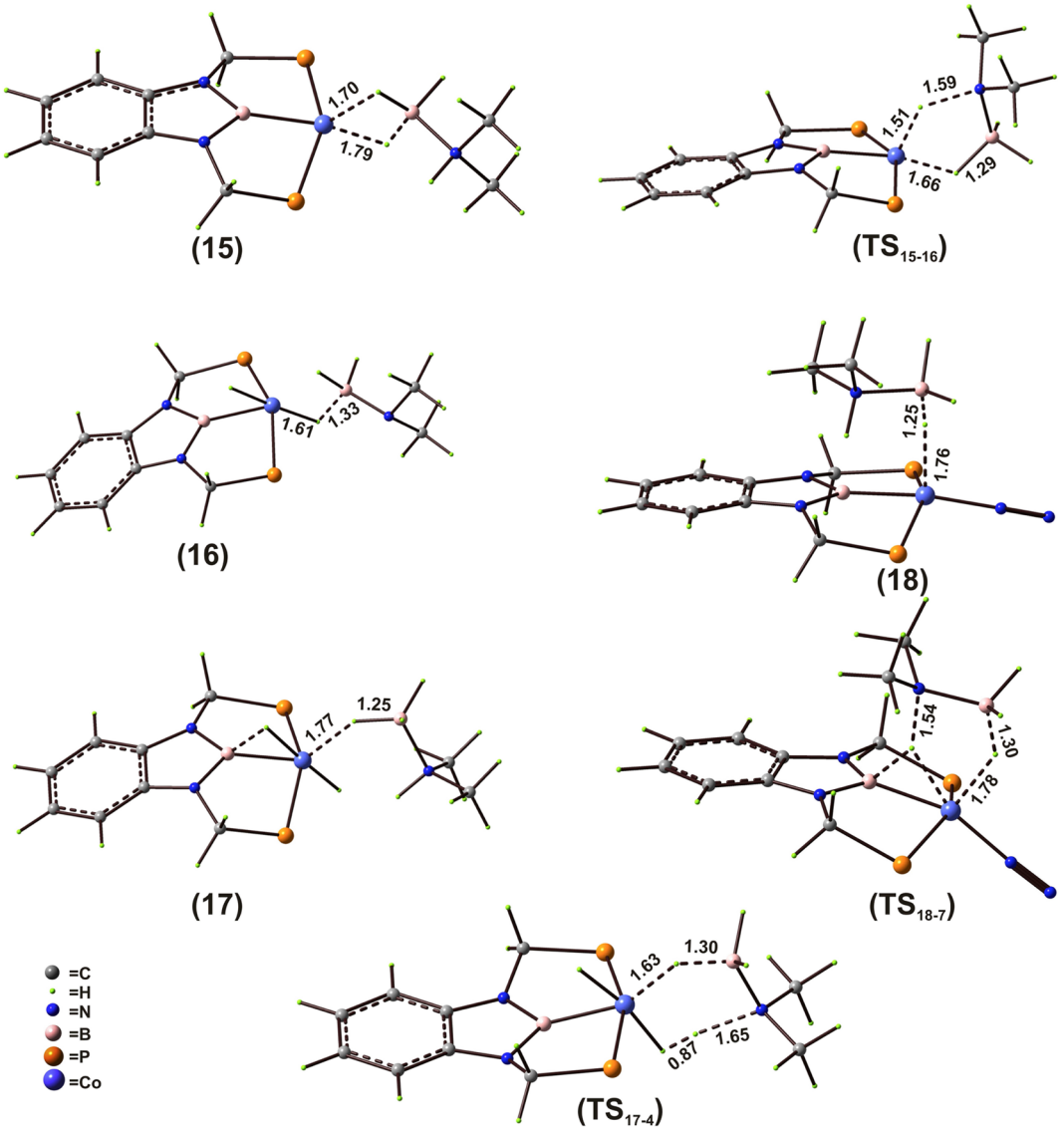

Figure 10. Optimized geometries of selected intermediates and transition states involved in Scheme 4. Key bond lengths are given in angstroms, and *tert*-butyl groups are omitted for clarity.

singlet entity, **15**. In **15**, we observe η^2 coordination of the BH_3 end of **AB** to the Co center (see Figure 10).

The generation of **15** from **1-N$_2$** is predicted to be exoergic by 1.5 kcal/mol, then the N−H proton in **15** gets transferred to the Co center by overcoming a free energy activation barrier of 25.0 kcal/mol and forms **16** (see Figure 11). The proton thus transferred occupies a bridging position between the B and Co. The change in free energy for the formation of **16** from **15** is exergonic by 13.0 kcal/mol. Compound **16** is an interesting intermediate because it has two possible fates hereon: it can serve as a template for further BN oligomer formation, as described by Bhunya et al. for oligomerization of $NH_2{=}BH_2$,[71] or alternatively, it can be seen as a $NMe_2{=}BH_2$ (**M**) coordinating to the $LCoH_2$ (**8**) moiety. Hence, **16** can dissociate into species **8** and $NMe_2{=}BH_2$ by surmounting a free energy barrier of 10.5 kcal/mol, and **8** thus generated can bind another amine−borane molecule, producing an intermediate **17**. From **17**, a concerted proton and hydride transfer event dehydrogenates the ligated **AB** molecule in **17** to produce a dihydrogenated Co species, **4**. This dehydrogenation pathway for **AB** is similar to those predicted for dehydrogenation of $NH_3{-}BH_3$ by Ir pincer catalyst[31] and NHC.[32] Transformation of **4** to **9** is a facile process via the formation of **5**, and self-dehydrogenation from **9** regenerates the catalytic active species **8** and H_2(g) (see Figure 4). Alternatively, **4** can undergo self-dehydrogenation and in the process regenerates **8** and H_2(g). Compound **8**, in turn, facilitates the catalytic dehydrogenation of **AB**. Thus, this is one of the plausible routes for dehydrogenation of amine−borane. On the other hand, in the presence of styrene, intermediate **8** can facilitate hydrogenation of the styrene, as has been discussed earlier. Dehydrogenation of amine−borane through the aforementioned channel has an overall RDB of 25.0 kcal/mol owing to the slow step of N−H activation in intermediate **15** to produce **16** through **TS$_{15-16}$**. In the process, **M** is formed catalytically.

(ii). Amine−Borane Associative Pathway. Alternatively, another mechanistic route exists in which the dehydrogenation process initiates through association of **AB** with the species **1-N$_2$** prior to N_2 dissociation, and the reaction occurs exclusively on the singlet surface (S = 0). Intriguingly, we have been able to locate an intermediate, **18**, in which the **AB** moiety can interact with the Co metal center in **1-N$_2$** with the hydride over

DOI: 10.1021/cs501359n
ACS Catal. 2015, 5, 2754−2769

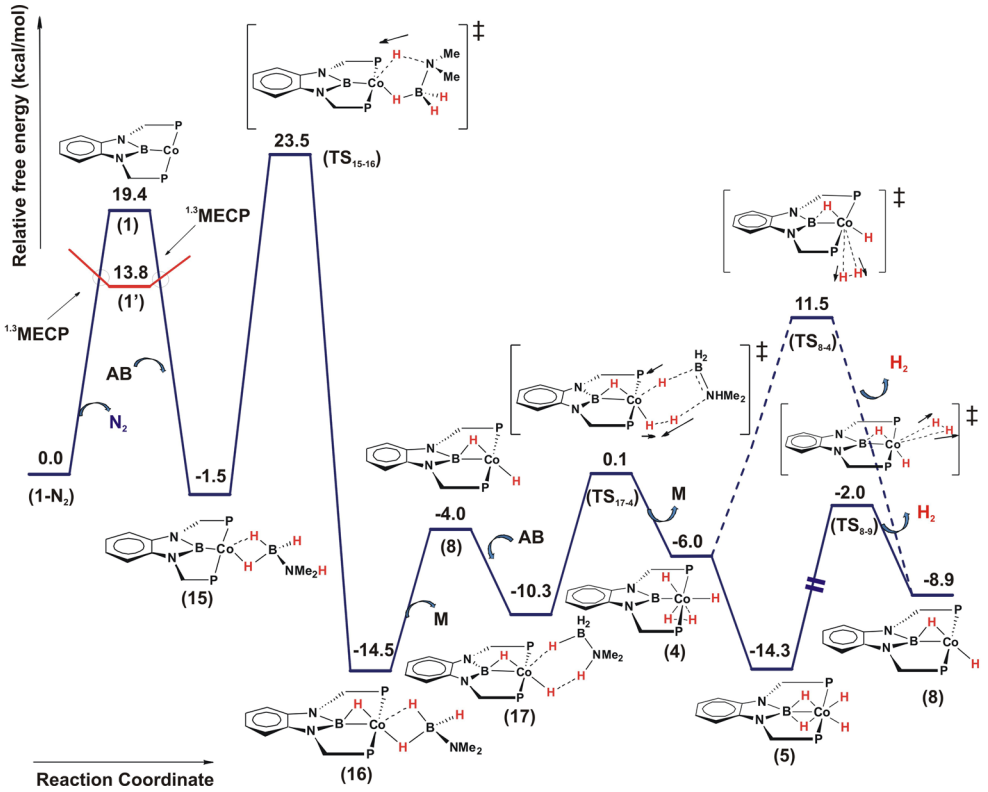

Figure 11. Free energy profile for N_2 dissociative route for amine−borane dehydrogenation. Red, triplet surface; blue, singlet surface.

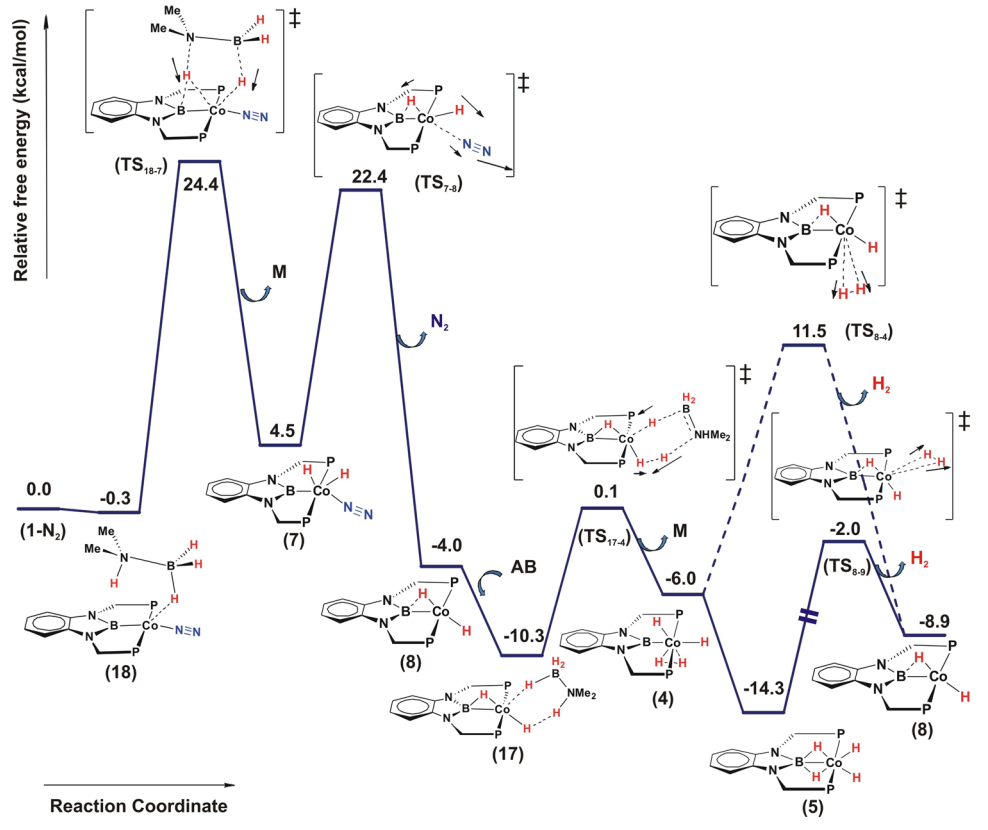

Figure 12. Free energy profile for **AB** associative route for amine−borane dehydrogenation.

the boron center. Subsequently, a concerted proton and hydride shift can happen ($\mathbf{TS}_{18-7}$) by overcoming a free energy activation barrier of 24.7 kcal/mol (see Figure 12). Compound 7, which was previously mentioned in the H_2 associative pathway, is thus generated in this step along with a free $NMe_2{=}BH_2$. As previously reported, N_2 dissociation from 7

DOI: 10.1021/cs501359n
ACS Catal. 2015, 5, 2754−2769

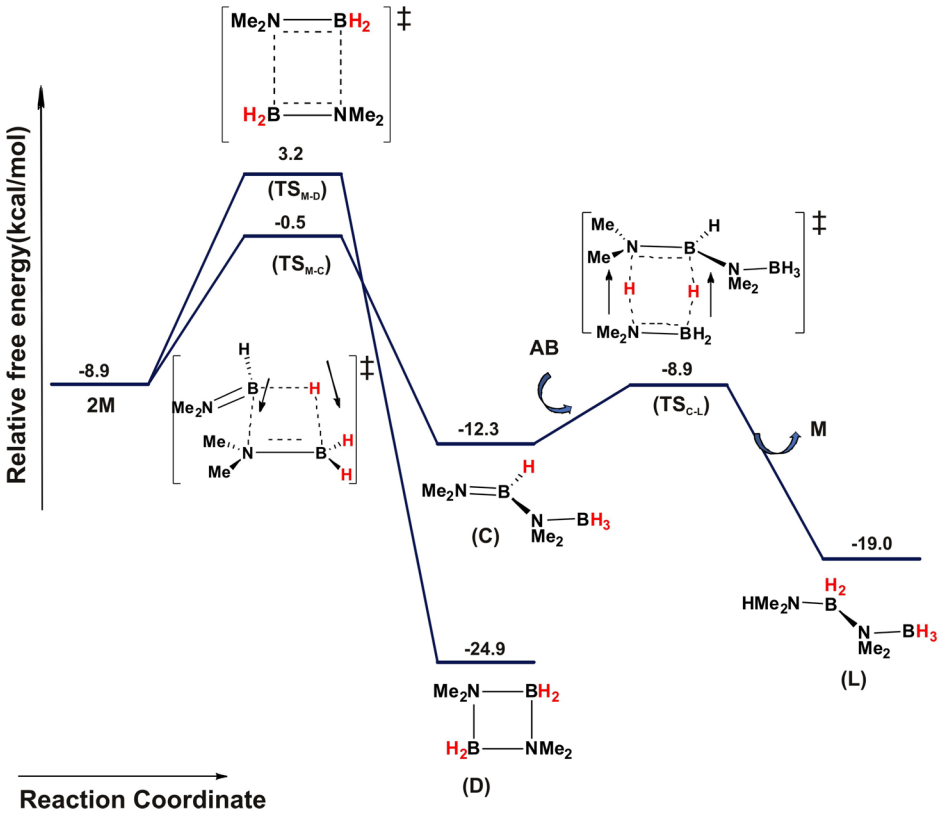

Figure 13. Free energy profile for off-metal amino−borane dimerization.

occurs via TS_{7-8} to give rise to **8**. The free energy of activation of TS_{7-8} is predicted to be 22.7 kcal/mol. Thus, the RDB for the formation of **8** is predicted to be 24.7 kcal/mol.

Hence, for all practical purposes, the formation of **8** happens through two competing channels: one through a N_2 dissociative channel with a RDB of 25.0 kcal/mol and the other through an **AB** associative pathway with a RDB of 24.7 kcal/mol. In both of the channels, **8** is produced with a moderately high barrier. The **AB** dehydrogenation barriers obtained with the B3PW91-GD3 functional are also moderately high and competing in nature (see the Supporting Information). Consequently, one may expect that the rate of formation of **8** would be slow at room temperature. As stated earlier, **8** can catalytically dehydrogenate **AB**, with a barrier of 10.4 kcal/mol. Peters et al. have reported that **AB** dehydrogenation takes ∼6 h for the formation of the cyclobutane analogue (**D**). Furthermore, by comparing the RDB of generation of **8** in the presence of molecular H_2(g) (RDB = 17.3 kcal/mol) and **AB** (RDB = 24.7 kcal/mol), one can easily conclude that olefin hydrogenation would be much faster in the presence of H_2(g) compared with that of **AB** dehydrogenation. Thus, our findings from the theoretical investigations are in good agreement with the experimental observations.[20]

Fate of in-Situ-Generated NMe_2═BH_2. We have investigated several possibilities for understanding the fate of in-situ-generated **M**. It can dimerize in the solvent without participation of the catalyst, or dimerization can occur at the metal center.

Off-metal dimerization of in-situ-generated **M** ensues through intermolecular $2\pi + 2\pi$ cycloaddition to form a cyclobutane analogue (**D**) with TS_{M-D}. The associated barrier for this process is predicted to be 12.1 kcal/mol. Competitively, two molecules of NMe_2═BH_2 can dimerize through a hydroboration reaction in which the B−H bond of one entity of **M** gets added across the B═N bond of another **M** via TS_{M-C} to form BH_3−NMe_2−BH═NMe_2 (**C**), as has also been predicted to happen for NH_2═BH_2 prior to oligomerization.[72,73] During the earlier stages of dehydrogenation of NMe_2H−BH_3, the intermediate **C** is likely to get hydrogenated by another NMe_2H−BH_3 through concerted proton and hydride transfer (TS_{C-L}), producing the linear butane analogue (**L**) and another molecule of NMe_2═BH_2, as predicted for the in situ dimerization of NH_2═BH_2 by Malakar et al.[74] Incidentally, the formation of the butane analogue is likely to be kinetically favorable; however, because **D** is much more thermodynamically stable than **L**, it is likely as the reaction progresses that the population of **L** would decrease because it would revert back to the more thermodynamically stable cyclobutane analogue through the reverse channel shown in Figure 13. Optimized geometries of all the intermediates and transition states involved in this reaction channel (Figure 13) are shown in Figure 14; hence, the product distribution is dictated by thermodynamic vs. kinetic control.

The linear butane analogue is the kinetically controlled product, and it is formed at a faster rate. Peters et al. reported that they observed a higher concentration of **L** (kinetically controlled product, RDB = 8.4 kcal/mol) in the reaction medium initially, and then it decreased with time and ultimately converted to **D** (thermodynamically controlled product, RDB = 12.1 kcal/mol). Alternatively, we have investigated metal-catalyzed reaction channels for the formation of the linear butane analogue and conversion of **L** to **D** (see the Supporting Information). Our computations reveal that the minimum energy path to dimerization on a metal center has a significantly higher RDB (24 kcal/mol) as compared with the barrier for off-metal dimerization (RDB = 12.1 kcal/mol). A similar trend is

DOI: 10.1021/cs501359n
ACS Catal. 2015, 5, 2754−2769

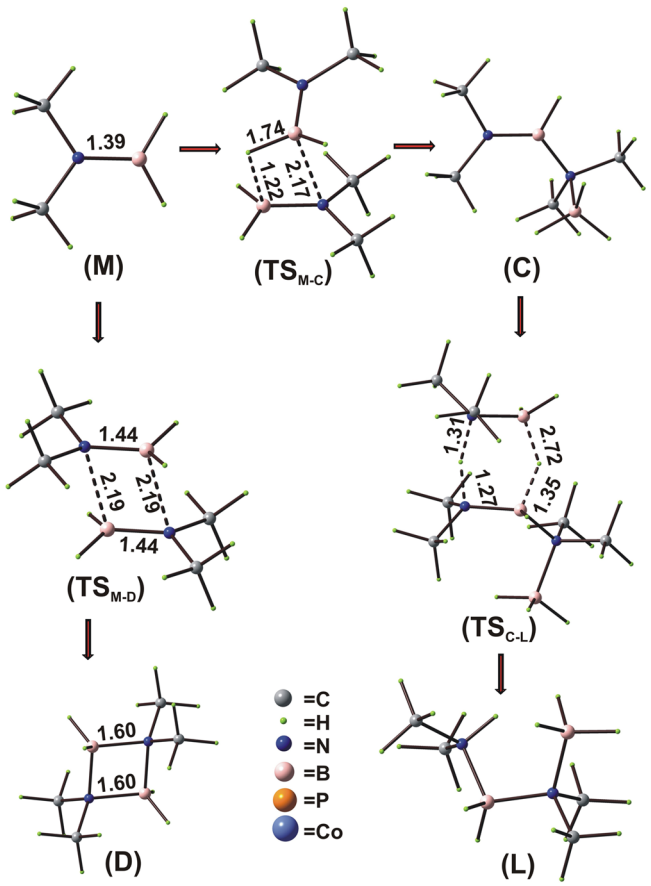

Figure 14. Optimized geometries of selected intermediates and transition states involved in Figure 13. Key bond lengths are given in angstroms.

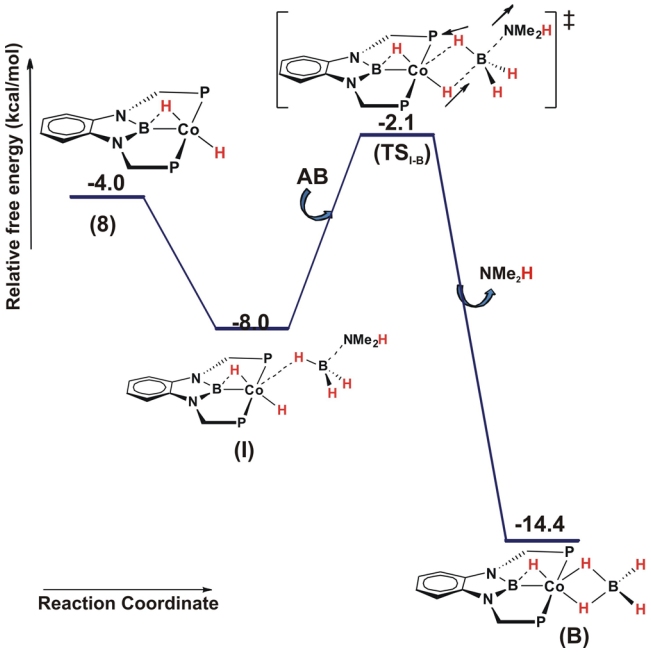

Figure 15. Proposed deactivation pathway of **8** in the presence of **AB**.

observed when we compare the barriers for **L** to **D** conversion in the metal-catalyzed and off-metal channels. Hence, we expect that the metal has limited role in the dimerization of **M** and formation of **L** and subsequent conversion of **L** to **D**.

Active Catalytic Species Deactivation Pathway in the Presence of Amine−Borane. We have also identified a deactivation pathway of the active catalytic species **8** that is the main obstacle of amine−borane dehydrogenation and transfer hydrogenation. Compound **8** forms a stable intermediate, **I**, in which the hydride end of **AB** interacts with the Co center. The NBO charge analysis of **8** (see Figure 6) clearly shows that the terminal hydrogen is hydridic in nature, which in turn can perform an intermolecular nucleophilic attack (S_N2) $\mathbf{TS_{I-B}}$ on the electron-deficient boron center of the amine−borane and forms a stable hydridoborane cobalt tetrahydridoborate complex (**B**).[20] The activation barrier of this nucleophilic attack is predicted to be 5.9 kcal/mol (see Figure 15).

Deactivation of **8** leads to reduction in the concentration of the active complex in the solution medium. The activation barrier for catalyst blocking being lesser in comparsion to amine−borane dehydrogenation and transfer dehydrogenation is predicted to be the major reason for the catalyst deactivation.This suggests the reason for the usage of excess strong bases, such as NEt_3, in the reaction mixture under the experimental conditions. Addition of excess NEt_3 ensures that the active catalytic form of the metal complex (**8**) is regenerated through nuleophilic (S_N2) attack on the B center of **I**, resulting in formation of free NEt_3−BH_3.

CONCLUDING REMARKS

In summary, we have conducted density functional theory (DFT) calculations with B3PW91-D functional to elucidate the mechanism for Co-boryl complex, $LCo(N_2)$, catalyzed: (i) hydrogenation of styrene, (ii) dehydrogenation of amine−borane, and (iii) transfer dehydrogenation of styrene using amine−borane. Our studies reveal that all three processes involve an active catalytic species, $LCo(H)_2$ (**8**). In the presence of H_2 pressure, the formation of the active catalytic species involves dissociation of N_2 from the parent complex. The reaction coordinate along the dissociation of N_2 from $LCo(N_2)$ involves crossing of the singlet electronic state with a low-lying triplet state, hence implicating a distinct role of switching of spin states in the active catalytic species generation. In the direct hydrogenation case, **8** is generated from the resting form of the catalyst, dihydrogenated Co species, **5**. We find that the boryl ligand has a noninncoent role in facilitating formation of **8** upon reacting of the Co species with **AB** in both of the low-lying channels disclosed in this work. The boron atom in the boryl ligand adjacent to the metal center directly participates in generation of the active catalytic species (**8**) for the transfer dehydrogenation using **AB** by facilitating formation of a bridged B−H−Co moiety.

The generation of active catalytic species $LCo(H)_2$ (**8**) for the **AB** dehydrogenation and transfer hydrogenation of olefin in the presence of **AB** through (i) N_2 dissociative and (ii) **AB** associative pathway are associated with higher activation barriers, 25.0 and 24.7 kcal/mol, respectively, compared with that of the generation of **8** in the presence of molecular H_2, which is predicted to be only 17.3 kcal/mol. In addition, there is an active catalytic species deactivation pathway in the presence of **AB** that further retards the transfer hydrogenation process. These are the primary reasons that explain the observed experimental observation that the catalyzed hydrogenation of styrene is much faster with H_2 as compared with the catalyzed transfer hydrogenation of styrene with **AB**.

DOI: 10.1021/cs501359n
ACS Catal. 2015, 5, 2754−2769

Moreover, in the transfer hydrogenation process, **AB** and **S** competitively bind to the active catalytic species **8**, thus further slowing down the overall hydrogenation of the olefin. Compound **8** can hydrogenate alkene through stepwise H transfer. The active catalytic species **8** dehydrogenates **AB** through concerted proton and hydride transfer for **AB** dehydrogenation and forms amino−borane and dihydrogenated species **5**, which can liberate H_2 with a very low activation barrier (12.3 kcal/mol) and regenerate **8**.

■ ASSOCIATED CONTENT

Supporting Information

The following file is available free of charge on the ACS Publications website at DOI: 10.1021/cs501359n.

Calculation method of the Gibbs free energy correction for gas phase entities, MECP geometries, metal-assisted formation pathway of **L** and metal-assisted conversion of **L** to **D**, B3PW91-D calculated thermal correction to enthalpy, thermal correction to Gibbs free energy, and Cartesian coordinates of all stationary points located in this work (PDF)

■ AUTHOR INFORMATION

Corresponding Author

*Phone: +91-33-2473 4971. E-mail: rcap@iacs.res.in.

Notes

The authors declare no competing financial interest.

■ ACKNOWLEDGMENTS

G.G thanks the Council of Scientific and Industrial Research (CSIR) India. A.P. thanks the Department of Science and Technology (DST) India.

■ REFERENCES

(1) Albrecht, M.; van Koten, G. *Angew. Chem., Int. Ed.* **2001**, *40*, 3750−3781.
(2) van der Boom, M. E.; Milstein, D. *Chem. Rev.* **2003**, *103*, 1759−1792.
(3) *The Chemistry of Pincer Compounds*; Elsevier: Oxford, U.K., 2007.
(4) Gottker-Schnetmann, I.; White, P.; Brookhart, M. *Organometallics* **2004**, *23*, 1766−1776.
(5) Tanaka, R.; Yamashita, M.; Nozaki, K. *J. Am. Chem. Soc.* **2009**, *131*, 14168−14169.
(6) Segawa, Y.; Yamashita, M.; Nozaki, K. *J. Am. Chem. Soc.* **2009**, *131*, 9201−9203.
(7) Hasegawa, M.; Segawa, Y.; Yamashita, M.; Nozaki, K. *Angew. Chem., Int. Ed.* **2012**, *124*, 7062−7066.
(8) Harman, W. H.; Peters, J. C. *J. Am. Chem. Soc.* **2012**, *134*, 5080−5082.
(9) Zeng, G.; Sakai, S. *Inorg. Chem.* **2013**, *52*, 2844−2853.
(10) Irvine, G. J.; Lesley, M. J. G.; Marder, T. B.; Norman, N. C.; Rice, C. R.; Robins, E. G.; Roper, W. R.; Whittell, G. R.; Wright, L. J. *Chem. Rev.* **1988**, *98*, 2685−2722.
(11) Waltz, K. M.; Hartwig, J. F. *Science* **1997**, *277*, 211−213.
(12) Segawa, Y.; Yamashita, M.; Nozaki, K. *Science* **2006**, *314*, 113−115.
(13) Waltz, K. M.; Muhoro, C. N.; Hartwig, J. F. *Organometallics* **1999**, *18*, 3383−3393.
(14) Parkin, G. *Organometallics* **2006**, *25*, 4744−4744.
(15) Landry, V. K.; Melnick, J. G.; Buccella, D.; Pang, K.; Ulichny, J. C.; Parkin, G. *Inorg. Chem.* **2006**, *45*, 2588−2597.
(16) Musaev, D. G.; Morokuma, K. *J. Phys. Chem.* **1996**, *100*, 6509−6517.
(17) Dickinson, A. A.; Willock, D. J.; Calder, R. J.; Aldridge, S. *Organometallics* **2002**, *21*, 1146−1157.
(18) Zhu, J.; Lin, Z.; Marder, T. B. *Inorg. Chem.* **2005**, *44*, 9384−9390.
(19) Cundari, T. R.; Zhao, Y. *Inorg. Chim. Acta* **2003**, *345*, 70−80.
(20) Lin, T.-P.; Peters, J. C. *J. Am. Chem. Soc.* **2013**, *135*, 15310−15313.
(21) Hamilton, C. W.; Baker, R. T.; Staubitz, A.; Manners, I. *Chem. Soc. Rev.* **2009**, *38*, 279−293.
(22) Keaton, R. J.; Blacquiere, J. M.; Baker, R. T. *J. Am. Chem. Soc.* **2007**, *129*, 1844−1845.
(23) Bluhm, M. E.; Bradley, M. G.; Butterick, R.; Kusari, U.; Sneddon, L. G. *J. Am. Chem. Soc.* **2006**, *128*, 7748−7749.
(24) Lin, T.-P.; Peters, J. C. *J. Am. Chem. Soc.* **2014**, *136*, 13672−13683.
(25) Baker, R. T.; Gordon, J. C.; Hamilton, C. W.; henson, N. J.; Lin, P.-H.; Maguire, S.; Murugesu, M.; Scott, B. L.; Smythe, N. C. *J. Am. Chem. Soc.* **2012**, *134*, 5598−5609.
(26) Kalidindi, S. B.; Indirani, M.; Jagirdar, B. R. *Inorg. Chem.* **2008**, *47*, 7424−7429.
(27) Sloan, M. E.; Staubitz, A.; Clark, T. J.; Russel, C. A.; Lloyd-Jones, G. C.; Manners, I. J. *J. Am. Chem. Soc.* **2010**, *132*, 3831−3841.
(28) Douglas, T. M.; Chaplin, A. B.; Weller, A. S.; Yang, X.; Hall, M. B. *J. Am. Chem. Soc.* **2009**, *131*, 15440−15456.
(29) Douglas, T. M.; Chaplin, A. B.; Weller, A. S. *J. Am. Chem. Soc.* **2008**, *130*, 14432−14433.
(30) Pons, V.; Baker, R. T. *Angew. Chem., Int. Ed.* **2008**, *47*, 9600−9602.
(31) Paul, A.; Musgrave, C. B. *Angew. Chem., Int. Ed.* **2007**, *119*, 8301−8304.
(32) Zimmerman, P. M.; Paul, A.; Zhang, Z.; Musgrave, C. B. *Angew. Chem., Int. Ed.* **2009**, *48*, 2201−2205.
(33) Yang, X.; Hall, M. B. *J. Am. Chem. Soc.* **2008**, *130*, 1798−1799.
(34) Ohno, K.; Luo, Y. *Organometallics* **2007**, *26*, 3597−3600.
(35) Keaton, R. J.; Blacquiere, J. M.; Baker, R. T. *J. Am. Chem. Soc.* **2007**, *129*, 1844−1845.
(36) Chaplin, A. B.; Weller, A. S. *Angew. Chem., Int. Ed.* **2010**, *49*, 581−584.
(37) Hohenberg, P.; Kohn, W. *Phys. Rev.* **1964**, *136*, B864−B871.
(38) Kohn, W.; Sham, L. J. *Phys. Rev.* **1965**, *140*, A1133−A1138.
(39) Frisch, M. J.; Trucks, G. W.; Schlegel, H. B.; Scuseria, G. E.; Robb, M. A.; Cheeseman, J. R.; Scalmani, G.; Barone, V.; Mennucci, B.; Petersson, G. A.; Nakatsuji, H.; Caricato, M.; Li, X.; Hratchian, H. P.; Izmaylov, A. F.; Bloino, J.; Zheng, G.; Sonnenberg, J. L.; Hada, M.; Ehara, M.; Toyota, K.; Fukuda, R.; Hasegawa, J.; Ishida, M.; Nakajima, T.; Honda, Y.; Kitao, O.; Nakai, H.; Vreven, T.; Montgomery, J. A.; Peralta, J. E.; Ogliaro, F.; Bearpark, M.; Heyd, J. J.; Brothers, E.; Kudin, K. N.; Staroverov, V. N.; Kobayashi, R.; Normand, J.; Raghavachari, K.; Rendell, A.; Burant, J. C.; Iyengar, S. S.; Tomasi, J.; Cossi, M.; Rega, N.; Millam, J. M.; Klene, M.; Knox, J. E.; Cross, J. B.; Bakken, V.; Adamo, C.; Jaramillo, J.; Gomperts, R.; Stratmann, R. E.; Yazyev, O.; Austin, A. J.; Cammi, R.; Pomelli, C.; Ochterski, J. W.; Martin, R. L.; Morokuma, K.; Zakrzewski, V. G.; Voth, G. A.; Salvador, P.; Dannenberg, J. J.; Dapprich, S.; Daniels, A. D.; Farkas, O.; Foresman, J. B.; Ortiz, J. V.; Cioslowski, J.; Fox, D. J. *Gaussian 09*, Revision A.02; Gaussian, Inc.: Pittsburgh, PA, 2009.
(40) Becke, A. D. *Phys. Rev. A* **1988**, *38*, 3098−3100.
(41) Becke, A. D. *J. Chem. Phys.* **1993**, *98*, 5648−5652.
(42) Perdew, J. P. In *Electronic Structure of Solids*, 91st ed.; Ziesche, P., Eschrig, H., Eds.; Akademie Verlag: Berlin, 1991.
(43) Burke, K.; Perdew, J. P.; Wang, Y. In *Electronic Density Functional Theory: Recent Progress and New Directions*; Dobson, J. F., Vignale, G., Das, M. P., Eds.; Plenum: New York, 1998.
(44) Osuna, S.; Swart, M.; Solà, M. *J. Phys. Chem. A* **2011**, *115*, 3491−3496.
(45) Grimme, S. J. *J. Comput. Chem.* **2004**, *25*, 1463−1473.
(46) Grimme, S. J. *J. Comput. Chem.* **2006**, *27*, 1787−1799.
(47) Cramer, C. J.; Truhlar, D. G. *Phys. Chem. Chem. Phys.* **2009**, *11*, 10757−10816.

DOI: 10.1021/cs501359n
ACS Catal. 2015, 5, 2754−2769

(48) Sousa, S. F.; Fernandes, P. A.; Ramos, M. J. *J. Phys. Chem. A* **2007**, *111*, 10439−10452.
(49) Tsuda, M.; Dy, E. S.; Kasai, H. *J. Chem. Phys.* **2005**, *122*, 244719-1−244719-7.
(50) Doux, M.; le Floch, P.; Jean, Y. *Eur. J. Inorg. Chem.* **2006**, 2035−2039.
(51) Tsuda, M.; Dino, W. A.; Nakanishi, H.; Kasai, H. *Chem. Phys. Lett.* **2005**, *402*, 71−74.
(52) Carreon-Macedo, J.-L.; Harvey, J. N. *J. Am. Chem. Soc.* **2004**, *126*, 5789−5797.
(53) Yan, L.; Seminario, J. M. *J. Phys. Chem. A* **2005**, *109*, 6628−6633.
(54) Steinmetz, M.; Grimme, S. *ChemistryOpen* **2013**, *2*, 115−124.
(55) Chakraborty, S.; Lagaditis, P. O.; Forster, M.; Bielinski, E. A.; Hazari, N.; Holthausen, M. C.; Jones, W. J.; Schneider, S. *ACS Catal.* **2014**, *4*, 3994−4003.
(56) Dolg, M.; Wedig, U.; Stoll, H.; Preuss, H. *J. Chem. Phys.* **1987**, *86*, 866. See also http://www.tc.uni-koeln.de/cgi-bin/pp.pl?language=en,job=getrefs for a complete reference list.
(57) Tomasi, J.; Mennucci, B.; Cammi, R. *Chem. Rev.* **2005**, *105*, 2999−3093.
(58) Barone, V.; Cossi, M. *J. Phys. Chem. A* **1998**, *102*, 1995−2001.
(59) Spickermann, C. *Entropies of Condensed Phases and Complex Systems*; Springer Theses; Springer: Berlin, 2010, pp 76−80, and references therein.
(60) Roy, L.; Mittal, S.; Paul, A. *Angew. Chem.* **2012**, *124*, 4228−4232.
(61) Roy, L.; Mittal, S.; Paul, A. *Angew. Chem., Int. Ed.* **2012**, *51*, 4152−4156.
(62) Bhunya, S.; Paul, A. *Chem.—Eur. J.* **2013**, *19*, 11541−11546.
(63) Grimme, S.; Antony, J.; Ehrlich, S.; Krieg, H. *J. Chem. Phys.* **2010**, *132*, 154104.
(64) Smith, K. M.; Poli, R.; Harvey, J. N. *New J. Chem.* **2000**, *24*, 77−80.
(65) Harvey, J. N. *Faraday Discuss.* **2004**, *127*, 165−177.
(66) Keogh, D. W.; Poli, R. *J. Am. Chem. Soc.* **1997**, *119*, 2516−2523.
(67) Green, J. C.; Jardine, C. N. *J. Chem. Soc., Dalton Trans.,* **1999**, 3767−3770.
(68) Decker, S. A.; Klobukowski, M. *J. Am. Chem. Soc.* **1998**, *120*, 9342−9355.
(69) Harvey, J. N.; Aschi, M.; Schwarz, H.; Koch, W. *Theor. Chem. Acc.* **1998**, *99*, 95−99.
(70) Hebden, T. J.; St. John, A. J.; Gusev, D. G.; Kaminsky, W.; Goldberg, K. I.; Heinekey, D. M. *Angew. Chem., Int. Ed.* **2011**, *50*, 1873−1876.
(71) Bhunya, S.; Malakar, T.; Paul, A. *Chem. Commun.* **2014**, *50*, 5919−5922.
(72) Zimmerman, P. M.; Paul, A.; Zhang, Z.; Musgrave, C. B. *Inorg. Chem.* **2009**, *48*, 1069−1081.
(73) Nutt, W. R.; McKee, M. L. *Inorg. Chem.* **2007**, *46*, 7633−7645.
(74) Malakar, T.; Roy, L.; Paul, A. *Chem.—Eur. J.* **2013**, *19*, 5812−5817.

DOI: 10.1021/cs501359n
ACS Catal. 2015, 5, 2754−2769